ECS Transactions, 80 (10) 703-710 (2017)
10.1149/08010.0703ecst ©The Electrochemical Society

Cu_2ZnSnS_4 Electrodeposition by Sulfurization of Metallic Precursors

G. Perelstein, M. Valdes, M. Vazquez*
División Electroquímica Aplicada, INTEMA, UNMdP-CONICET, Mar del Plata
B7608FDQ, ARGENTINA

*corresponding autor: mvazquez@fi.mdp.edu.ar; tel: +54 223 4816600

This work describes the electrodeposition of a Cu-Zn-Sn precursor on conducting glass that transforms into Cu_2ZnSnS_4 during a heat treatment at 500 °C in vaporized sulfur. Citrate and hydroxyl concentrations were adjusted to fix the pH value in 5.9, so that Cu_2ZnSnS_4 could be deposited on top of ZnO in solar cells built in superstrate configuration. The deposits were characterized by X-ray diffraction, Raman spectroscopy, scanning electronic microscopy, UV-Vis spectroscopy and photoelectrochemical techniques. Cu_2ZnSnS_4 films obtained with short electrodeposition times are good-quality, p-type absorbers suitable to be used in kesterite thin films solar cells. The most promising results were obtained using 0.1 mol L^{-1} sodium citrate, which is attributed to a higher Zn content in the precursor deposit.

1. Introduction

Cu_2ZnSnS_4 (CZTS) is likely to replace $CuInGaSe_2$ (CIGS) as absorbing layer in thin films solar cells. CZTS has a high absorption coefficient and a direct bandgap energy value (E_{gap}) (1, 2). In addition, it is formed by elements that are non-toxic and abundant in the Earth crust. CZTS films deposited by solution-based methods constitute attractive candidates to build cost-effective and environmentally-friendly solar cells (3-7).

Several non-vacuum deposition methods are available. Among them, electrodeposition is particularly interesting, as it is easily transferred to industry (8).

Colombara et al. have summarized the main electrochemical methods appropriate for CZTS (9). In the so-called co-electrodeposition approach a Cu-Zn-Sn precursor (CZT) is deposited in a first stage. Later, sulfur is incorporated by reactive annealing in a sulfur-rich atmosphere to finally transform this precursor film into CZTS (10-16).

Many variables have to be fine-tuned with the purpose of obtaining a high-quality film, as needed for solar cell prototypes. Some of them are analyzed in this investigation, particularly the pH of the precursor bath. When CZTS films are deposited bearing in mind the construction of solar cells in superstrate configuration, CZTS has to be electrodeposited on top of an n-type transparent layer (in our case ZnO, work in progress). With this purpose, the optimal pH for the CZTS electrodeposition is 5.9 to prevent the dissolution of amphoteric ZnO. Different strategies to adjust the pH, such as NaOH and sodium citrate addition produce CZTS films with diverse properties, which are compared and analyzed.

Citrate ions are alkaline but they are also strong complexing agents, which may affect the concentration of the electroactive cations.

2. Experimental

A conventional three-electrode cell was used, with Pt as counter electrode and a saturated calomel electrode (SCE) as reference electrode. A PGZ 101 Voltalab® potentiostat controlled current and voltage.

Squares (20 x 20 mm^2) of conductive glass (fluorine-doped tin oxide, FTO, ρ=8 Ω sq^{-1}, thickness = 2 mm) were used as substrate, after cleaning them with detergent and isopropylic alcohol.

The precursor solution included copper, zinc and tin ions (PS3). PS3 consisted of 0.03 mol L^{-1} $CuSO_4$, 0.1 mol L^{-1} $ZnSO_4$, 0.01 mol L^{-1} $SnSO_4$ and 0.1 mol L^{-1} sodium citrate ($Na_3C_6H_5O_7$, NaCit) that serves as complexing agent. Sulfur is incorporated into the CZT ternary precursors by annealing the films in a sulfur-rich vapor atmosphere. The pH of the solution needs to be set to 5.9 so that, when used to construct solar cells, CZTS can be deposited on top of amphoteric ZnO (17). This can be achieved by either: a) adding NaOH or b) increasing NaCit concentration to 0.4 mol L^{-1}. This precursor solution is labeled as PS3-0.4.

CZT thin films were electrodeposited form PS3 and PS3-0.4 purged with N_2 and keeping the potential at -1.15 V during 10 min. The films were rinsed with distilled water. After drying, the deposits were thermally treated in the presence of sulfur powder using a home-built reactor, described earlier (18). The samples remained at 500 °C for 1 hour, and were then left to cool down naturally.

The films were analyzed by X-ray diffraction, scanning between 15° and 80°, with a PANalytical X'Pert PRO diffraction system and Cu-*Kα* radiation at 40 kV and 40 mA with a step size of 0.01°. Scanning electron microscopy (SEM) was carried out with a JEOL JSM-6460LV. The thickness of the films was measured with a KLA TENCOR D-100 profilometer. Raman spectra were recorded using an Invia Reflex confocal Raman microprobe using a 20x objective. 514 and the 785 nm lasers were used. Raman maps were built by probing a square region of interest (80 x 80 μm) and a 50x objective. 25 spectra were recorded in the x and y directions with 20 μm steps. The band gap energy (E_{GAP}) was calculated from transmission spectra recorded with a Shimadzu UV-3600 Plus spectrophotometer, with FTO as reference.

3. Results and discussion

The diffractograms of CZT precursors electrodeposited in PS3 and PS3-0.4 are presented in Figure 1. The patterns are dominated by SnO_2 peaks from the substrate (PDF 77-0452), but Sn (PDF 04-0673), Cu_5Zn_8 (PDF 71-0397, only present in PS3) and $Cu_{5.6}Sn$ (PDF 17-0865) are also detected. The intermetallic compounds have been reported before (15, 19). The peaks are sharper and more intense in PS3.

X-ray diffractograms of CZTS films prepared by annealing CZT are presented in Figure 2. CZT films effectively transform into CZTS with kesterite structure (PDF 26-0575). The peaks are quite narrow, particularly for PS3. This is expected as a result from the heat

treatment and indicates an improvement in the crystalline degree. The diffractograms show almost no evidence of secondary phases being formed during annealing, except for a very small signal that can be associated to $Cu_{2-x}S$ (PDF 02-1292) or to Cu_2S (PDF 03-1071).

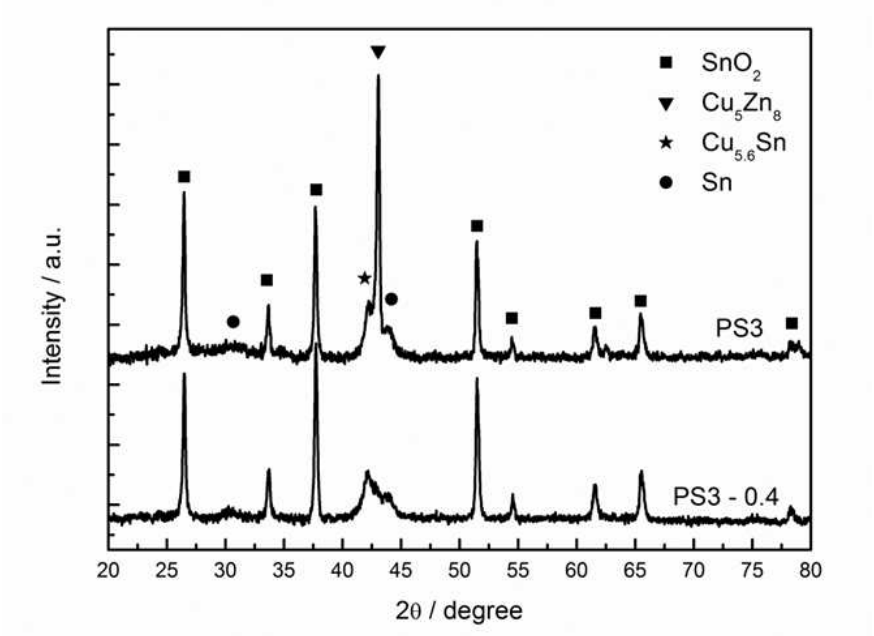

Figure 1. XRD corresponding to as-deposited CZT films electrodeposited using PS3 and PS-0.4 as precursor baths.

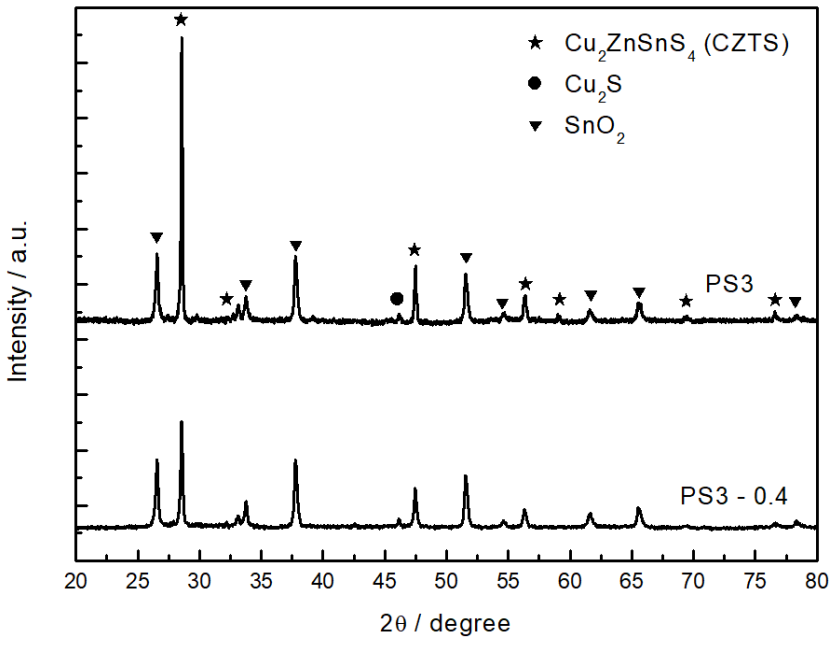

Figure 2. XRD corresponding to annealed CZTS films electrodeposited using PS3 and PS-0.4 as precursor baths.

Raman spectroscopy complements XRD structural analysis and may help to detect secondary phases. Figures 3a and 3b show Raman spectra of annealed films prepared from PS3 and PS3-04 using as excitation signal a 514 nm laser. Figures 3c and 3d present Raman maps, recorded using a 785 nm laser. The peaks were fitted with Lorentzian curves. Comparing Figures 3a and 3b, and regardless of the precursor solution, both spectra contain the main vibrational modes of the kesterite structure. When using the 514 laser, these are the A1 principal mode that can be seen at 338 cm^{-1} and the E(TO/LO) mode at 288 cm^{-1} (20, 21). The spectrum in Figure 3a also shows weak bands at 259 and 370 cm^{-1} that can be related to low intensity E and B symmetry modes. The bands are broader and poorly defined when using PS3-04, which can be taken as an indication of a lower crystalline degree.

With the 785 nm laser, the excitation wavelength is close to the bandgap energy of CZTS, which can enhance the Raman vibration signals. The maps in Figures 3c and 3d show that the composition each sample is homogenous throughout the whole surface. The maps also show that independently of the laser employed, the condition that uses PS3 as precursor solution produces higher quality CZTS films after sulfurization. These maps were recorded following the grid presented in Figure 3e, using 20 μm steps in the x and y directions.

Slupska and Ozga (22) investigated in detail the influence of citrate ions on the electrodeposition of Sn-Zn-Cu alloys. They found that higher citrate concentrations lead to a decrease in the concentration of the electroactive zinc(II) citrate complex ($ZnHCit^-$) near the electrode surface and, simultaneously, to an increase in the concentration of a non-electroactive zinc(II) citrate complex. Lower Zn content in the precursor deposit could then be responsible for the differences found in Figures 1, 2 and 3 between PS3 and PS3-04.

Figure 4 displays SEM micrographs of samples deposited using both precursor baths. There is good coverage and homogeneous grain size in both cases. The grain size is bigger when the deposit is prepared from PS3, which is desirable for photovoltaic applications, since grain boundaries can act as recombination centers. The thickness is similar in both cases, with values close to 1 μm.

The optical evaluation of sulfurized deposits prepared from PS3 and PS3-04 precursors is presented in Figure 5. The transmittance spectra can be transformed into $(\alpha h\nu)^2$ versus $(h\nu)$ plots, from which band gap energy (E_{gap}) values of the deposits can be calculated. E_{gap} values result in 1.63eV for PS3 and 1.58 eV for PS·-0.4. These values are in agreement with those reported in the literature for CZTS films (1).

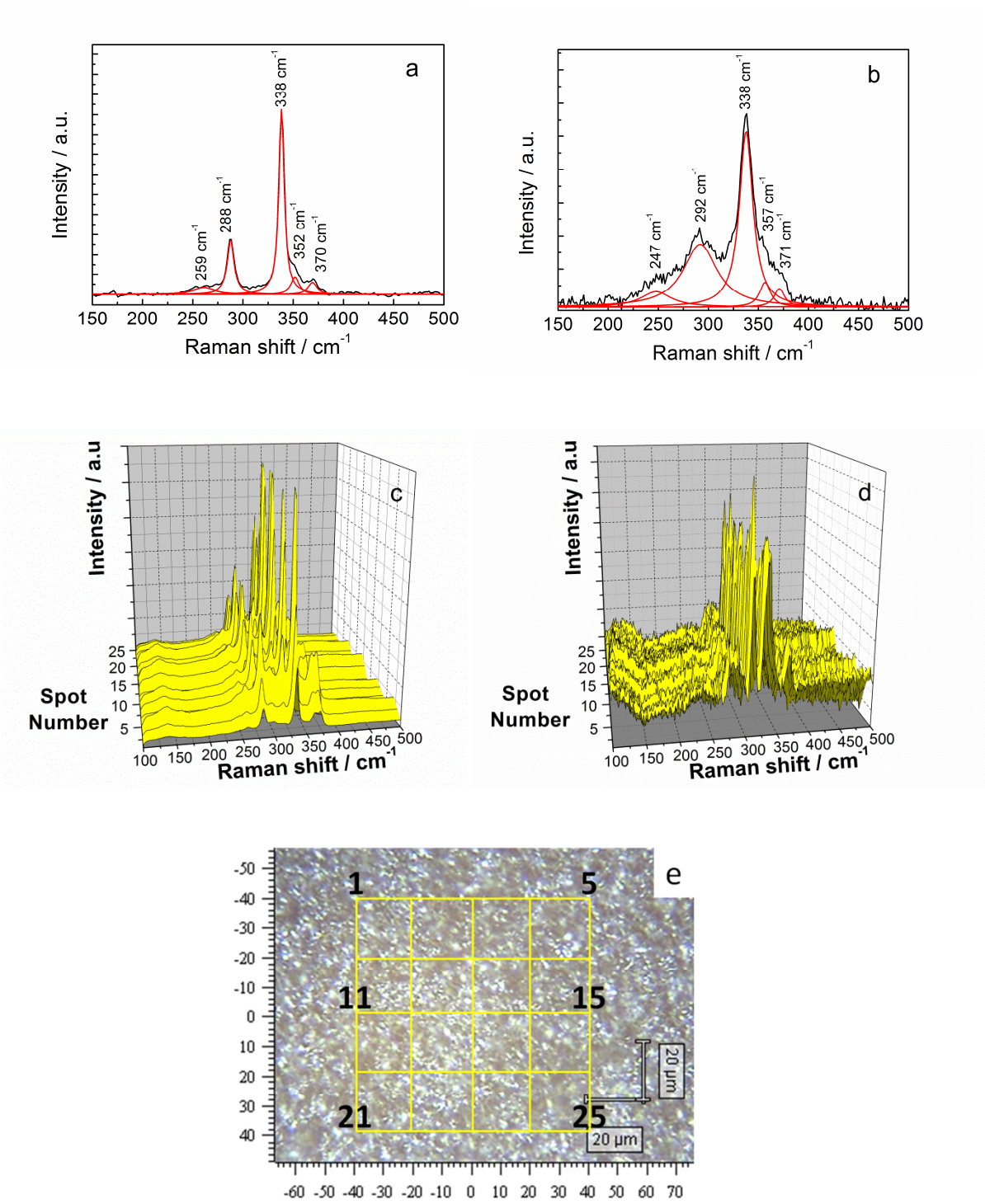

Figure 3. Raman spectra corresponding to annealed CZTS films electrodeposited using: a) PS3 as precursor baths and the 514 nm laser; b) PS3-04 as precursor bath and the 514 nm laser ; c) PS3 as precursor bath and the 785 nm laser; d) PS3-04 as precursor bath and the 785 nm laser; e) Grid used to record the maps shown in Figure 3c and 3d.

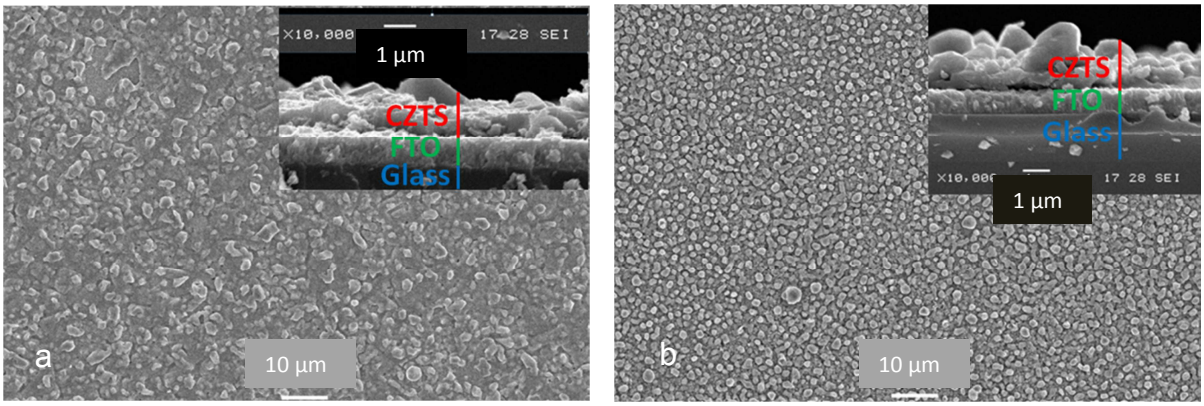

Figure 4. SEM micrographs sowing annealed CZTS films electrodeposited using as precursor baths: a) PS3; b) PS3-04.

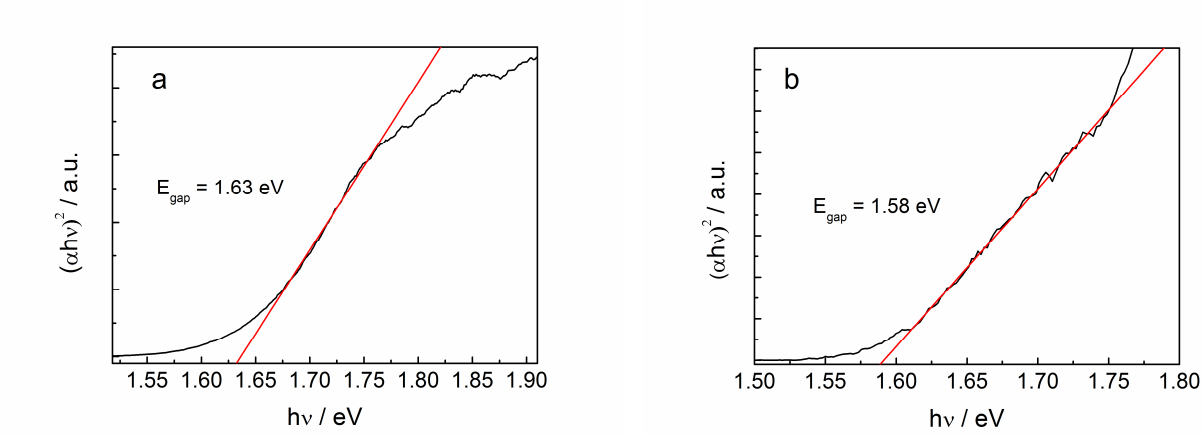

Figure 5. Plots of $(\alpha h\nu)^2$ vs. $(h\nu)$ recorded form annealed CZTS films electrodeposited using different precursor baths. a) PS3; b) PS3-04.

The photoelectrochemical properties of CZTS have also been investigated, in order to confirm that holes are the majority carriers. Photocurrent can be detected even at open circuit potential (OCP), by shinning chopped radiation on the semiconducting films. Electrons and holes move in opposite directions, reducing the potential difference across the space charge layer. CZTS is a p-type semiconductor, and so its Fermi level decreases when the band edge level bends downwards across the space charge layer. In this case, a negative photocurrent is recorded when (photo)generated electrons move towards the electrode/electrolyte interface, as shown in Figure 6. The negative (cathodic) nature of the photocurrent is expected for a p-type semiconductor. The time response is observed to be better when using PS3 as precursor bath and may also be related to a lower Zn content in the precursor CZT deposit. In addition, the shape of the photocurrent transient (quadrature of the on/off pulse) is better defined in the PS3 film. According to the results reported by Dale et al. (23) in their study of semiconducting $CuInSe_2$, this is an indication of lower

surface recombination of photogenerated carriers in comparison with the PS3-04, and therefore to a higher material quality of PS3 films.

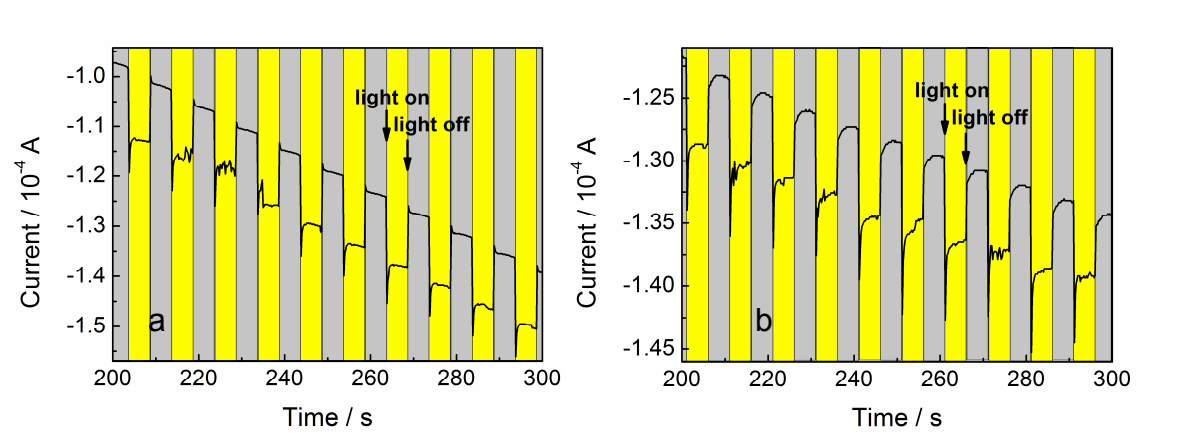

Figure 6. Photocurrent response of annealed CZTS films polarized at -0.7 V and electrodeposited using (a) PS3 and (b) PS3-04 as precursor baths. The electrodes were immersed in 0.1 mol L^{-1} Na_2SO_4 solution at pH 2.3, using chopped light (5 s on / 5 s off).

Conclusions

Raman spectroscopy and XRD results confirmed the formation of crystalline CZTS after sulfurization, with almost no secondary phases detected in the film.

Photocurrent analysis confirmed the p-type nature of the semiconductor.

Direct energy gap values close to 1.6 eV were estimated for CZTS films using transmittance spectra and correspond to good-quality CZTS.

Both samples show good coverage degree and similar thicknesses.

CZTS films obtained at pH 5.9 with short electrodeposition times are appropriated absorbers suitable to be used in kesterite thin films solar cells. The citrate content has a noticeable effect on the overall quality of the sulfurized film. The best results were obtained with the lowest citrate concentration and are probably related to the proportion of Zn in the precursor deposit.

Acknowledgments

The financial support from CONICET (PIP 0175), ANPCyT (PICT 972/15) and Universidad Nacional de Mar del Plata (ING477/16) is greatly acknowledged. G. Perelstein is also indebted to CONICET for providing his doctoral grant.

References

1 . K. Ito and T. Nakazawa, Japanese Journal of Applied Physics, Part 1: Regular Papers and Short Notes and Review Papers **27** 2094-2097 (1988).

2 . S. Siebentritt and S. Schorr, Progress in Photovoltaics: Research and Applications **20** 512-519 (2012).

3 . S. Kim, K.M. Kim, H. Tampo, H. Shibata, K. Matsubara and S. Niki, Solar Energy Materials and Solar Cells **144** 488-492 (2016).

4 . C.J. Hages, M.J. Koeper and R. Agrawal, Solar Energy Materials and Solar Cells **145** 342-348 (2016).

5 . X. Fu, Z. Ji, C. Li and Z. Zhou, Journal of Alloys and Compounds **688** 1013-1018 (2016).

6 . K. Cheng, J. Meng, X. Wang, Y. Huang, J. Liu, M. Xue and Z. Du, Materials Chemistry and Physics **163** 24-29 (2015).

7 . Q. Tian, Y. Cui, G. Wang and D. Pan, RSC Advances **5** 4184-4190 (2015).

8 . Y.D. Gamburg and G. Zangari, Theory and Practice of Metal Electrodeposition, Springer New York (2011).

9 . D. Colombara, A. Crossay, L. Vauche, S. Jaime, M. Arasimowicz, P.P. Grand and P.J. Dale, Physica Status Solidi (A) Applications and Materials Science **212** 88-102 (2015).

10 . A. Ennaoui, M. Lux-Steiner, A. Weber, D. Abou-Ras, I. Kötschau, H.W. Schock, R. Schurr, A. Hölzing, S. Jost, R. Hock, T. Voß, J. Schulze and A. Kirbs, Thin Solid Films **517** 2511-2514 (2009).

11 . H. Araki, Y. Kubo, K. Jimbo, W.S. Maw, H. Katagiri, M. Yamazaki, K. Oishi and A. Takeuchi, Physica Status Solidi (C) Current Topics in Solid State Physics **6** 1266-1268 (2009).

12 . Y. Wang, J. Ma, P. Liu, Y. Chen, R. Li, J. Gu, J. Lu, S.E. Yang and X. Gao, Materials Letters **77** 13-16 (2012).

13 . K.V. Gurav, S.M. Pawar, S.W. Shin, M.P. Suryawanshi, G.L. Agawane, P.S. Patil, J.H. Moon, J.H. Yun and J.H. Kim, Applied Surface Science **283** 74-80 (2013).

14 . K.D. Lee, S.W. Seo, D.K. Lee, H. Kim, J.H. Jeong, M.J. Ko, B. Kim, D.H. Kim and J.Y. Kim, Thin Solid Films **546** 294-298 (2013).

15 . Y. Li, T. Yuan, L. Jiang, Z. Su and F. Liu, Journal of Alloys and Compounds **610** 331-336 (2014).

16 . M. Dimitrievska, A. Fairbrother, E. Saucedo, A. Pérez-Rodríguez and V. Izquierdo-Roca, Solar Energy Materials and Solar Cells **149** 304-309 (2016).

17 . L. Wang, D.-B. Li, K. Li, C. Chen, H.-X. Deng, L. Gao, Y. Zhao, F. Jiang, L. Li, F. Huang, Y. He, H. Song, G. Niu and J. Tang, **2** 17046 (2017).

18 . M. Valdés, Y. Di Iorio, K. Castañeda, R.E. Marotti and M. Vázquez, Journal of Applied Electrochemistry 1-11 (2017).

19 . T. Hreid, J. Li, Y. Zhang, H.J. Spratt, H. Wang and G. Will, RSC Advances **5** 65114-65122 (2015).

20 . T. Gürel, C. Sevik and T. ÇağIn, Physical Review B - Condensed Matter and Materials Physics **84** 205201 (2011).

21 . X. Fontané, V. Izquierdo-Roca, E. Saucedo, S. Schorr, V.O. Yukhymchuk, M.Y. Valakh, A. Pérez-Rodríguez and J.R. Morante, Journal of Alloys and Compounds **539** 190-194 (2012).

22 . M. Slupska and P. Ozga, Electrochimica Acta **141** 149-160 (2014).

23 . P.J. Dale, A.P. Samantilleke, G. Zoppi, I. Forbes, S. Roncallo and L.M. Peter, ECS Transactions **6** 535-546 (2007).